

GADER: GAit DEtection and Recognition in the Wild

Yuxiang Guo, Cheng Peng, Ram Prabhakar,
Chun Pong Lau, Rama Chellappa
Johns Hopkins University, Baltimore, MD, USA

{yguo87, cpeng26, rprabha3, clau13, rchella4}@jhu.edu

Abstract

Gait recognition holds the promise of robustly identifying subjects based on their walking patterns instead of color information. While previous approaches have performed well for curated indoor scenes, they have significantly impeded applicability in unconstrained situations, e.g. outdoor, long distance scenes. We propose an end-to-end GAit DEtection and Recognition (GADER) algorithm for human authentication in challenging outdoor scenarios. Specifically, GADER leverages a Double Helical Signature to detect the fragment of human movement and incorporates a novel gait recognition method, which learns representations by distilling from an auxiliary RGB recognition model. At inference time, GADER only uses the silhouette modality but benefits from a more robust representation. Extensive experiments on indoor and outdoor datasets demonstrate that the proposed method outperforms the State-of-The-Arts for gait recognition and verification, with a significant 20.6% improvement on unconstrained, long distance scenes.

1. Introduction

Unconstrained biometric identification, e.g., in outdoor and far-away situations, has been a longstanding challenge [51, 50, 36, 37]. RGB-based face and body recognition systems focus on learning discriminating *spatial* features; however, effects like challenging view angles, low face resolution, changing appearances (e.g., clothes and glasses), and long distance turbulence are observed in the real world and can significantly disrupt spatial information. Consequently, the RGB-based recognition systems tend to perform inconsistently in unconstrained scenarios.

Gait analysis provides an alternative modality for human recognition by intentionally masking away the color information and focusing on learning discriminating features in the *temporal* domain. As such, it is potentially more robust to challenging, unconstrained situations, and has been broadly applied in many applications such as surveillance [4], health [12] and crime analysis [15], etc.

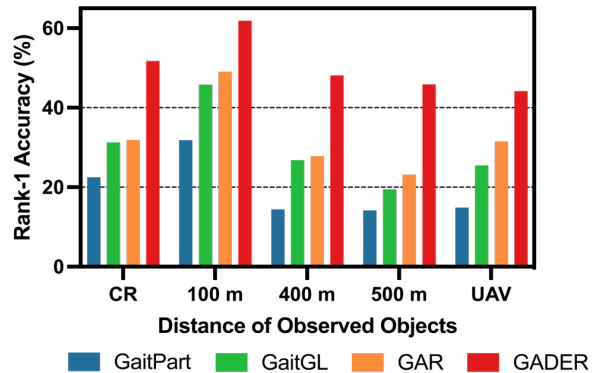


Figure 1: Compared to other gait recognition models, GADER has significant improvement, especially increases 26.38% at 500m, in outdoor recognition at various distances. Close Range(CR), Unmanned Aerial Vehicle(UAV).

The field of gait recognition has been significantly bloomed [35, 16, 10, 26, 1, 36] by traditional methods, including template matching methods [5, 28, 48] and model-based methods [3, 46, 7, 24], but limited by dependency on the scale and viewing angle and being sensitive to video quality, respectively. Deep learning (DL)-based approaches [9, 2, 27] have made significant advances compared to traditional methods. They are able to generate robust identity embeddings by directly processing the complex temporal information present in gait sequences. This enables effective recognition under sources of variability, such as changes in viewpoint and clothing, making DL-based methods widely used in these years.

While DL-based gait recognition performs well for indoor scenes, it often fails to achieve good performance in unconstrained/outdoor scenarios. In this work, we seek to apply gait recognition to unconstrained situations with minimum data curation. The recently collected BRIAR [11] dataset contains standing, structured walking, and random walking sequences, which mimic the real-world constraints of gait recognition. Existing gait recognition methods assume that the subject is always walking with periodic move-

ment and that there are no standing sequences. By making such assumption, these methods tend to learn suboptimal representation, e.g. achieving only 31% on close range recognition. This highlights the need for an approach to filter out non-walking sequences and make the gait recognition inputs more consistent.

Current silhouette-based methods employ the practice of *size normalization*, where input silhouettes are resized to the same resolution regardless of the subject’s distance from the camera, can lead to information loss. Particularly, the sequence of the ratio between the original body chip and the normalized one can implicitly offer important viewpoint information, which is useful for generating effective embeddings [8]. Unfortunately, this cue is lost in the resizing operation. Besides, RGB modality is often overlooked in gait recognition due to privacy concerns and potential biases introduced by clothing. However, RGB images contain rich information that can be used to build robust features that cannot be captured by silhouettes alone. By solely referring to the feature space of the RGB modality in the training step, we are able to protect the privacy of individuals while still taking advantage of the discrimination provided by RGB images.

In this paper, we aim to push the frontiers of unconstrained gait analysis through an end-to-end GAit Detection and Recognition system in the wild (GADER). To address the problem of mixing the moving and standing sequences, we introduce a novel gait detection module (Figure 4) that detects the walking and non-walking parts of a sequence. Instead of using a 3D volume to capture the dynamic movement, our gait detector uses the reliable Double Helical Signature (DHS) [34, 32], a 2D gait pattern with a lightweight classification model to distinguish the walking portion of the input sequence from others. Specifically, we do not input the entire gait pattern into the model. Instead, we split the signature into multiple windows of varying lengths to get predictions, followed by Non-Maximum Suppression (NMS), to localize the movement duration. This provides a pure gait sequence for existing gait recognition models, making it suitable for real-world scenarios.

For the gait recognition module (GAR), along with the size normalized silhouettes, we embed the ratio of change in size from the original body size as an attention signal. This *ratio attention* helps preserve the viewpoint information that is beneficial for robust identity representation. We further introduce a *cross-modality feature distillation* step, where we guide intermediate gait features to be more expressive by making them more similar to features generated from RGB frames. This enables the gait features to maintain their robustness against appearance changes, while also benefiting from the discriminative power of RGB features. The augmented gait features can be obtained from silhouettes and do not require the presence of RGB frames during

inference.

In summary, GADER introduces three contributions:

- We introduce a light-weight gait detector to automatically detect clips with human movements and avoid learning on static information.
- We propose a novel gait recognition model, which leverages the color space and size information during training; specifically, knowledge distillation on RGB features is used to enhance feature space capacity.
- We conduct a series of evaluations, i.e. rank retrieval and verification on CASIA-B Gait3D and BRIAR datasets, and show superior performance than the state-of-the-art means.

2. Related Work

Traditional Gait Representations: Traditional gait recognition methods can be classified into appearance-based and human model-based. Appearance based gait systems use input data without making any assumptions on human body model [35, 10, 48]. Bobick and Davis [5] proposed Motion Energy Image (MEI) and Motion History Image (MHI) to model the input silhouette sequence as a template. Han and Bhanu [16] introduced Gait Energy Image (GEI) template as an average of aligned and normalized silhouette frames. In [28], Liu and Zheng improved GEI and proposed Gait History Image (GHI). GHI is generated from silhouettes that combines both static and dynamic or temporal characteristics. While appearance-based methods are simple and fast, they are view and scale dependent.

Model-based methods represent whole human body using well-defined models and use them to represent gait. The methods vary by the different techniques used for modeling human body, such as hidden Markov models [22, 30], stride length and walking tempo [3], stick figures [46], multi-part [7, 24], inter body part distances [6, 41], joint angles [40], and Velocity Hough Transform [31] among many.

Deep Learning-based Methods: Early deep learning-based methods learn global gait representation using information like silhouettes [9], GEI [38, 43, 18], and body pose [26, 1, 2] as input to CNNs. The GaitSet [9] model applies horizontal pyramid mapping on a set of features extracted from individual silhouette frames to obtain efficient gait representation. Alternatively, local representations extracted using part-based methods have shown success in recent years [27, 49, 29]. GaitPart [13] uses focal convolution on different body parts and aggregates them using micro-motion capture module. Several methods have been proposed to combine global and local features. One such method by Lin *et al.* [27] aggregates local temporal information while retaining spatial information. Subsequently, global and local features extraction followed by temporal pooling is applied to generate robust gait features. Recently, Guo *et al.* [14] utilize both RGB and silhouette data to ex-

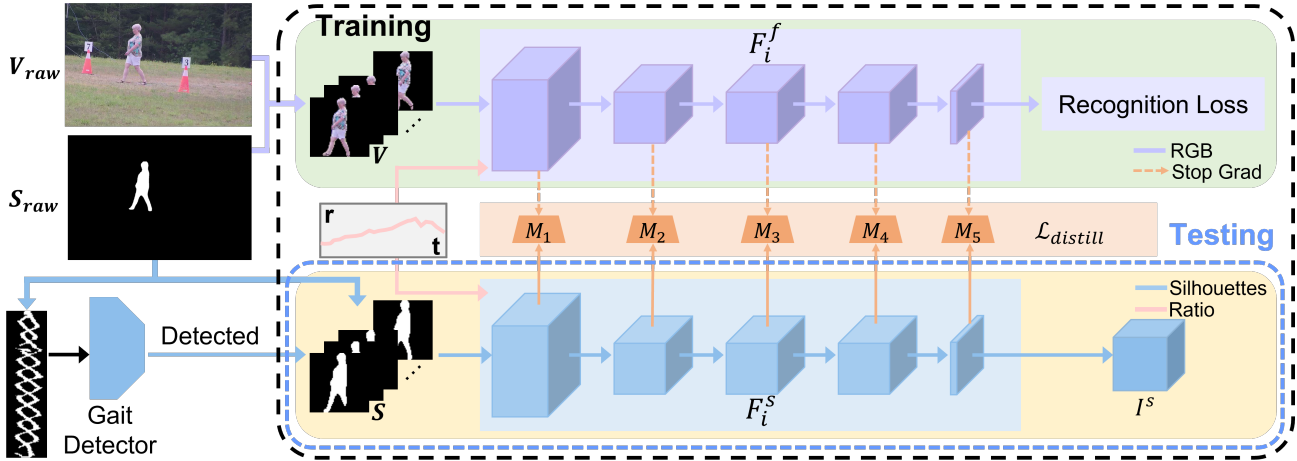


Figure 2: Overview of our proposed end-to-end pipeline. GADER consists of two parts: gait detection and gait recognition, i.e. GAR. The gait detector utilizes gait representation to filter out unqualified sequences. GAR leverages ratio attention and RGB feature space to extract a more robust silhouette feature for recognition.

tract robust gait features for challenging indoor and outdoor sequences. In [8], Chai *et al.* used Lagrange’s equation to demonstrate the importance of second order motion information in gait recognition.

Recognition in the Wild: Developing an accurate gait representation in the wild is a long term goal and has been broadly researched over the past decade. Towards that aim, Zhu *et al.* curated a large scale gait dataset called GREW [51]. It is a natural videos dataset consisting of 128K sequences of 26K identities captured over 882 cameras. Similarly, Zheng *et al.* [50] collected Gait3D dataset that contains silhouettes, 2D/3D keypoints, and 3D meshes for 3D gait recognition. The authors [50] observed that state-of-the-art gait recognition methods do not translate similar superior performance in GREW and Gait3D as they do in indoor dataset like CASIA-B. Due to privacy concern, both GREW and Gait3D datasets are silhouette based and do not contain the corresponding RGB sequences. Also, unlike the BRIAR dataset, GREW and Gait3D do not contain sequences captured at long distances (500m). Hence, they do not address challenges due to atmospheric turbulence. Another research direction includes enhancing images captured at long distance and use the restored images for recognition [45, 23]. In [23], Lau *et al.* proposed a generative model that deblurs and removes turbulence effects for face recognition at distance. Such methods have not been explored for gait recognition.

3. Method

In this work, we focus on silhouette-based gait recognition, which relies on the binary masks of the subjects in a video. Formally, we denote a video as a 4D tensor, i.e. $V \in \mathbb{R}^{H \times W \times T \times 3}$, where H, W, T are the height, width,

and frame index. For each frame t , the subject silhouette $s_t \in \{0, 1\}^{H \times W}$ is obtained from an off-the-shelf segmentation model, e.g. [42]. Gait recognition takes $S = [s_t]_{t=1}^T$ as the input, and obtains corresponding features $f = F_\theta(S)$ from a feature extractor F_θ . Triplet loss [17] is used to constrain the training process of F_θ with respect to ground-truth labels $y \in \{1, 2, \dots, |\mathcal{Y}|\}$ for each video in the training sets, where $|\mathcal{Y}|$ is the cardinality of the label set. After F_θ is trained, gallery gait silhouettes S^g and probe gait silhouettes S^p are passed into F_θ to obtain the gait feature f^g and f^p . To recognize the probe identity, a similarity metric \mathcal{D} , such as Euclidean distance or cosine similarity, is used to find $\mathcal{D}(f^g, f^p)$, where the gallery subject g and the probe p will be regarded as the same person if they are the most similar in feature space.

In the following sections, we introduce GAit DETection and Recognition in the Wild (GADER), designed for gait recognition in the wild. GADER has two parts: a gait detector model, which uses 2D gait representations to detect human movements in a video, and a gait recognition model, which incorporates resizing information and is guided by a teacher feature space from an RGB-based recognition model during training.

3.1. Gait Detector

Previous gait recognition methods [9, 13, 27, 25, 8] directly use silhouettes S as the input, under the assumption that the video sequence captures *the entire body* and *constant movement*. While these assumptions are for curated datasets, such as CASIA-B [47], OU-MVLP [39], and GREW [51], they are often untrue for unconstrained videos and will lead to suboptimal learning if left untreated [19]. To this end, we propose a gait detector to assess if the video sequence contains gait movement with the complete body,

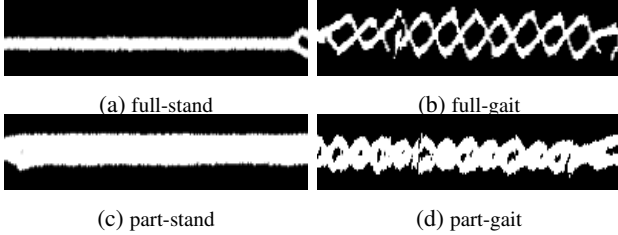


Figure 3: The four cases of DHS(a-d) are shown using two variables: full/part - indicates whether the body is complete, and stand/gait - shows whether gait appears.

similar to the role of face detection in face recognition.

3.1.1 Gait Representation

To make the gait detector compatible with silhouette-based methods, we extract a gait representation based on normalized silhouette \mathcal{S} . An ideal gait representation should be able to discriminate moving subjects from stationary ones and partial body from full body. Since the legs of the body have periodic movement and contribute significantly to gait recognition, we use the Double Helical Signature (DHS) [34]. DHS is a classic gait representation that captures the movement of the knee to describe gait movement as a function of time. As our input \mathcal{S} is normalized to the same size, we can deduce the knee height $\mathcal{H}_{\text{knee}}$ to be approximately a quarter of the overall height. By taking a slice from the silhouette sequence, i.e., $\mathcal{S}_{\text{knee}}(x, t) = \mathcal{S}(x, \mathcal{H}_{\text{knee}}, t)$, $\mathcal{S}_{\text{knee}} \in \mathbb{R}^{W \times T}$, we can obtain a double helical structure that indicates human movement.

As shown in Figure 3, the DHS pattern is rather discriminating. For the standing case, the DHS pattern shows a constant straight line since there is no movement at knees. When the subject is walking, a periodic pattern is obtained, known as a type of ‘‘Frieze pattern’’ [32]. Given an incomplete body, DHS appears rather different as $\mathcal{H}_{\text{knee}}$ does not correspond to the knee position anymore; consequently, DHS becomes thicker.

3.1.2 Light-weighted Classification

Unconstrained human motion naturally involves a variety of movements, including turning, standing, and walking within a short period of time. This can result in DHS sequences that contain multiple walking fragments. During the training step, we randomly select the start point and duration from the whole DHS and get R_{knee} . Each segment has the same height as DHS’s. After that, the fragment is processed by a five-layer Convolutional Neural Network \mathcal{M}_{ϕ} to get the feature. To handle the varying window lengths, we introduce a temporal pooling module in the form of a max-pooling layer to generate a window-length invariant embedding. Then, we use a four-class multi-layer perceptron (MLP) to obtain the prediction, and the cross entropy

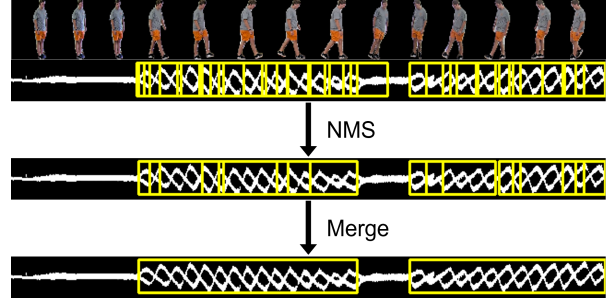


Figure 4: Frames with gait information are not always present in a video clip. We introduce a gait detector leveraging a DHS followed by NMS and merge to locate the place where gait information is present in a sequence. The yellow bounding boxes are the detected gait clips. loss is applied between the prediction(H) and ground-truth to get a gait classification model.

$$H = \text{MLP}(\mathcal{P}_{\text{Max}}^{1 \times 1 \times t}(\mathcal{M}_{\phi}(R_{\text{knee}}))), \quad (1)$$

where $\mathcal{P}_{\text{Max}}^{1 \times 1 \times t}$ represents temporal pooling module with size $(1 \times 1 \times t)$, and t is the window’s width.

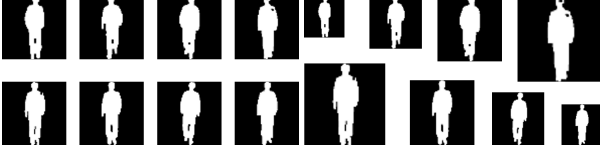
To identify and localize these fragments, in the inference time, we first split the entire DHS sequence into multiple windows of varying durations R_{knee}^n , where n represents the number of windows. Each window goes through the well-trained gait classification model and gets a corresponding prediction. We only keep the complete body gait predictions and reduce the overlapping by Non-Maximum Suppression (NMS). Finally, we check the reduced windows’ inner distance and concatenate them if the distance is smaller than a predefined threshold. And the ratio of the detected movement length to the entire DHS sequence serves as an indicator for determining whether the sequence should be further utilized in the gait recognition module. The process is illustrated in Figure 4. Thus our gait detector automatically identifies the corresponding movement status of each clip.

3.2. GAit Recognition (GAR)

With the help of the gait detector, we can obtain relatively clean gait sequences for gait recognition. In the recognition stage, we propose GAR, which incorporates prior knowledge such as the RGB feature space and the resizing information. The architecture is shown in Figure 2.

3.2.1 Ratio Attention

The *resizing ratio* is defined as the change in size from the original bounding box to the normalized silhouette shape, which is usually $64 \times 64 \times T$. Intuitively, the resizing ratios are similar if two videos are recorded from the same viewpoint. As such, these ratios naturally encode viewpoint information, as shown in Figure 5. Viewpoint information has



(a) Normalized input without ratio (b) Normalized input with ratio
 Figure 5: In each subfigure, the upper row of silhouettes are collected from 0° and the lower ones from 180° . It is hard to distinguish normalized silhouettes from different angles (5a). But they are critical when the ratio is introduced (5b).

been shown to improve gait recognition performances [8]; however, such information is difficult to obtain in unconstrained situations, especially when the subject’s movement is not monotonic. In this work, we leverage resizing ratios to represent changing views.

To effectively incorporate ratios into the gait feature extraction module, we apply it as an attention mechanism and fuse it into the network. The ratios are embedded using 1D convolution $F_{1DCConv}$, followed by a sigmoid function $Sigmoid(*)$, i.e.:

$$r = Sigmoid(F_{1DCConv}(\frac{S_{raw}}{S})), \quad (2)$$

where S_{raw} and S are the body bounding boxes in the original and standardized silhouette, and $r \in \mathbb{R}^{1 \times 1 \times T}$.

3.2.2 Cross Modality Distillation

Previous works [13, 9, 27, 25, 44] have shown that silhouette-based recognition is robust to appearance changes such as different clothing and low image quality. On the flip side, segmenting RGB frames into silhouettes leads to a loss in useful information, e.g. the rich texture information. While gait recognition systems do not have access to color space information at *test time*, they can be benefited by learning from the feature space learned by an RGB-based recognition system *during training* to better separate identities. To this end, GAR introduces an auxiliary recognition branch to extract features from RGB images. We denote $F_{3DCConv}^f, F_{3DCConv}^s$ as the first 3D convolution layers to the RGB and silhouette feature extraction backbones. Combining with ratio attention r , GAR first obtains weight features, i.e.

$$\mathbf{F}_1^f = r * F_{3DCConv}^f(\mathbf{V}), \mathbf{F}_1^s = r * F_{3DCConv}^s(\mathbf{S}), \quad (3)$$

After that, we apply the rest of backbones to the processed features,

$$\begin{aligned} \mathbf{F}_{i+1}^f &= F_i^f(\mathbf{F}_i^f), \mathbf{F}_{i+1}^s = F_i^s(\mathbf{F}_i^s), \\ I^f &= F_N^f(\mathbf{F}_N^f), I^s = F_N^s(\mathbf{F}_N^s), \end{aligned} \quad (4)$$

in which I^f and I^s are identification embedding, and $i \in \{1, 2, \dots, N\}$ is the convolution block index. Triplet

loss [17] is applied to enlarge the similarity of representations from different subjects and minimize the ones from the same identity for both modalities.

$$\begin{aligned} \mathcal{L}_{tri}^f &= [\|I^f - I_-^f\|_2 - \|I^f - I_+^f\|_2 + m]_+, \\ \mathcal{L}_{tri}^s &= [\|I^s - I_-^s\|_2 - \|I^s - I_+^s\|_2 + m]_+, \end{aligned} \quad (5)$$

where the superscript $+$ and $-$ in the identification embedding represent the same and different subject to I^f respectively. m is the margin of the triplet loss, and operation $[*]_+$ describes $\max(*, 0)$.

A cross-modal distillation loss is introduced within GAR, which promotes the representation power of gait features based on the learned RGB feature space. While one possible design is to directly constrain the silhouette/RGB features to be similar, we find this approach to be suboptimal. Since both modalities have their specific discriminative advantages, forcing their features to be similar leads to an averaged representation that does not benefit from the specificity from each modality. As we focus on obtaining expressive features from silhouettes, an additional convolutional layer C_i is introduced for the i -th intermediate silhouette feature \mathbf{F}_i^s , such that the transformed features are constrained to be similar to \mathbf{F}_i^f . This cross-modality distillation loss can be described as:

$$\mathcal{L}_{distill} = \sum_i (\mathcal{D}(\varnothing(\mathbf{F}_i^f), C_i(\mathbf{F}_i^s))), \quad (6)$$

where stop gradient (\varnothing) operation is used such that the RGB branch is not affected by the silhouette features in this process. Note that C_i is only used at training time. Overall, the training loss is

$$\mathcal{L}_{train} = \lambda_f \mathcal{L}_{tri}^f + \lambda_s \mathcal{L}_{tri}^s + \lambda_{distill} \mathcal{L}_{distill}, \quad (7)$$

where $\lambda_{f,s,distill} = 0.425, 0.425, 0.15$ are the loss hyperparameters used during training.

4. Experiments

4.1. Datasets and Metric

In this work, we focus on applying gait recognition to unconstrained scenarios with minimum data curation. To this end, the **BRIAR** [11] dataset, as shown in Figure 6, is used extensively. BRIAR consists of 577 and 639 subjects used as training and test sets, respectively. In the test set, there are 354 distractors and 285 target subjects. For each identity, there are both indoor (*controlled*) and outdoor (*field*) sequences. The *controlled* set is collected with 10 cameras from different viewing angles to record structure and random walking. In the *field* set, the sequences are collected at varying distances and altitudes, namely close range (CR),



Figure 6: Examples of subjects in different conditions from the BRIAR dataset at different distances attitudes and clothing. The columns represent controlled-set1, controlled-set2, CR-stand, CR-walk, 100m, 400m, 500m and UAV respectively. Samples are in the **supplementary material** section.

100m, 400m, 500m and unmanned aerial vehicle (UAV). There are also videos consisting of subjects standing all the time in the field set, as shown in Figure 6. For each subject, two garment settings are applied, i.e. set1 and set2. The duration of each video is approximately 90 seconds. Human silhouettes are obtained using Detectron2 [42]. Compared to other unconstrained datasets, BRIAR takes 1. outdoor atmospheric turbulence, 2. different walking status and 3. incomplete body shapes into consideration, making it very challenging.

Similar to previous methods for gait recognition, we also evaluate the proposed approach on **CASIA-B** [47], a controlled, indoor dataset with periodic motion obtained. CASIA-B consists of 124 subjects with three walking conditions which are normal walking (NM), walking with a bag (BG) and walking in a coat or jacket (CL). Each sequence consists of eleven view points ranging from 0° to 180° at an interval of 18° . We divide the dataset into training and test sets according to the widely applied protocol outlined in [43]. To further demonstrate the effectiveness of the proposed approach in the unconstrained case, we also test GADER on the **Gait3D** [50] dataset. It consists of 25,309 sequences recorded by 39 cameras on 4,000 subjects inside a large supermarket. We follow the official data split, taking the 1,000 subjects as the test set in cross-domain evaluation. In the test set, each subject has one sequence as a query and the rest serve as the gallery.

Evaluation Metric For CASIA-B and BRIAR, *verification* and *rank retrieval* are used to evaluate gait recognition. For verification, the gallery sequences are paired with probe

sequences. We measure the performance using Receiver-Operating Characteristics (ROC) curves that plot the True Accept Rate (TAR) as a function of the False Accept Rate (FAR). As for Gait3D, the evaluation protocol follows the open-set instance retrieval setting and calculates the average Rank-1 and 5 accuracies, mean Average Precision (mAP), and mean Inverse Negative Penalty (mINP) over all queries.

4.2. Implementation Details

All experiments are implemented in Pytorch [33] with four NVIDIA A5000 GPUs. We follow [9] to obtain normalized silhouettes and RGB body chips at the resolution of 64×64 from the original segmentation masks and frames for CASIA-B and BRIAR. The resizing ratio is recorded during the normalization process. For CASIA-B, we use GaitGL [27] as the backbone for RGB and silhouette feature extraction. For the BRIAR dataset, we use a larger GaitGL architecture designed for OU-MVLP [39], considering the number of identities and scene complexity. In the training phase, the batch size for both datasets is (8,8), i.e. eight subjects with eight videos per subject for each batch. Thirty continuous frames are randomly sampled from a video.

Our gait detector is trained using DHS generated from the BRIAR training set in a supervised manner using annotations provided by BRIAR. To ensure robustness to varying time duration, we randomly select input lengths ranging from 30 to 100 for each training iteration. The detector is evaluated on DHS from the testing sets of three datasets. Specifically, we select window sizes of 33, 50, and 80. The gait detection performance is evaluated using average accuracy, where correctness means 50% or more of the sequence has predictions matching with the ground truth. CASIA-B and Gait3D are pure gait datasets, and we suppose all sequences in these datasets as complete body gait.

4.3. Quantitative Evaluation

Evaluation on CASIA-B [47] We compare our proposed gait recognition method with current arts, including GaitPart [13], GaitGL [27], 3DLocal[21], CSTL [20], Lagrange [8] on CASIA-B. The Rank-1 accuracy is in Table 1.

Compared to other methods, our model achieves similar performance on NM and BG compared to Lagrange [8] and better performance on CL. Overall, our method outperforms Lagrange [8], CSTL [20], and 3DLocal [21] by 0.2%, 0.7% and 0.5%, respectively. We note that GAR improves overall performance from 91.8% to 92.6% compared to the original GaitGL with only an extra 1D convolution to extract ratio information in the test phase. GADER even further increases the accuracy to 92.9% with the help of the gait detector.

We also evaluate the *verification* performance. The TAR(%) results are shown in Table 2. Our proposed method

Gallery NM#1-4		0° – 180°											
Probe		0°	18°	36°	54°	72°	90°	108°	126°	144°	162°	180°	mean
CL#1-2	GaitPart [13]	70.7	85.5	86.9	83.3	77.1	72.5	76.9	82.2	83.8	80.2	66.5	78.7
	GaitGL [27]	76.6	90.0	90.3	87.1	84.5	79.0	84.1	87.0	87.3	84.4	69.5	83.6
	3DLocal [21]	78.5	88.9	91.0	89.2	83.7	80.5	83.2	84.3	87.9	87.1	74.7	84.5
	CSTL [20]	78.1	89.4	91.6	86.6	82.1	79.9	81.8	86.3	88.7	86.6	75.3	84.2
	Lagrange [8]	77.4	90.6	93.2	90.2	84.7	80.3	85.2	87.7	89.3	86.6	71.0	85.1
	GAR	80.8	90.5	92.2	91.0	84.7	79.7	84.8	89.6	89.7	87.1	72.8	85.7
GADER	82.5	90.5	92.0	91.9	85.2	79.3	84.5	89.8	89.8	87.1	72.3	85.9	
Overall	GaitPart [13]	84.6	93.0	94.3	92.3	86.5	83.2	87.2	91.3	93.0	90.6	80.9	88.8
	GaitGL [27]	88.4	94.9	95.3	93.5	91.7	87.9	91.1	94.1	94.9	93.3	85.0	91.8
	3DLocal [21]	89.1	94.6	96.1	94.7	91.2	87.5	90.7	93.2	94.8	94.5	86.1	92.1
	CSTL [20]	89.0	94.9	95.9	93.3	89.7	87.8	90.3	93.6	95.0	93.6	87.3	91.9
	Lagrange [8]	89.1	94.9	96.3	94.7	91.8	88.3	91.4	94.5	95.5	94.1	85.6	92.4
	GAR	90.2	95.0	95.9	94.7	91.9	88.2	91.5	94.9	95.5	94.1	86.2	92.6
GADER	91.9	95.2	96.0	95.6	91.9	88.0	91.4	94.9	95.7	94.1	86.8	92.9	

Table 1: Rank-1 accuracy (%) on CASIA-B excluding identical-view case for CL#1-2 and overall. The complete table is included in the **supplementary material** section.

Models	NM	BG	CL	Mean
GaitPart [13]	90.5	78.7	64.2	77.8
GaitGL [27]	91.05	82.69	66.60	80.11
GAR	91.48	83.07	67.94	80.83
GADER	92.33	84.50	69.80	82.21

Table 2: Verification (TPR(%)@FPR= $1e^{-2}$) on CASIA-B.

Probe	CR	100m	400m	500m	UAV	Mean
GaitPart [13]	22.48	31.81	14.42	14.18	14.85	19.55
GaitGL [27]	31.26	45.82	26.81	19.49	25.48	29.77
GAR	31.88	49.06	27.81	23.17	31.57	32.70
GADER	51.78	61.88	48.11	45.87	44.19	50.37
FAR	$1e^{-4}$	$1e^{-3}$	$1e^{-2}$	$1e^{-1}$		
GaitPart [13]	4.04	11.33	27.47	59.39		
GaitGL [27]	9.15	18.64	35.21	62.67		
GAR	8.50	18.97	35.28	63.46		
GADER	14.72	31.06	61.68	90.47		

Table 3: Rank-1 accuracy (%) and verification on BRIAR. CR stands for Close Range, i.e. below 100m; Unmanned Aerial Vehicle (UAV).

outperforms GaitGL and GaitPart by 0.72% and 3.03% overall, attaining 80.83%. And our method also achieves the best performance in NM, BG and CL with 91.48%, 83.07% and 67.94%. It is noticeable that although the recognition results in NM and BG are likely saturated, there is still room for improvement on the verification task.

Evaluation on BRIAR [11] To demonstrate the superior performance of the proposed methods in the wild, we further evaluate on BRIAR with GaitPart [13] and GaitGL [27]. The Rank-1 accuracy is shown in Table 3. Our gait recognition model achieves the highest overall recognition performance, reaching 50.37%, and is 20.6% and 30.82% higher than GaitGL and GaitPart. It is also higher

than GAR by 17.67%, just showing that it is beneficial to apply the gait detector to eliminate sequences without human movements. GAR still leads to better performance than previous arts, indicating that the referred discriminative feature space from RGB and ratio information contribute to a better silhouette feature.

When it comes to *verification*, the TAR (%) results are shown Table 3. Compared to GaitGL, our method increases by 26.47%, achieving 61.68% when FAR= $1e^{-2}$. From Table 3, we observe a big improvement when the gait detector is included. The recognition system’s verification results increase from 35.28% to over 60% when FAR= $1e^{-2}$. This indicates that gait recognition will perform reasonably well if only the qualified gait sequences are used as input.

Evaluation on Gait3D [50] To evaluate our model on a public outdoor dataset, we also did cross-domain evaluation on Gait3D. The results are in Table 4. We see that our proposed method achieves higher performance in all criteria. Especially, Rank-1 increases 3.5% to 25.02%. Since cross-domain evaluation is a challenging task, the results are lower than single-domain ones. It is worth noting that, we also adopt GaitGL [27] for the cross-domain evaluation using CASIA-B, OUMVLP, GREW and BRIAR for train and testing on Gait3D. The model trained on the BRIAR dataset exhibited superior performance compared to the others, indicating that the complexity of BRIAR dataset confers greater generalization ability to the trained model.

Gait Detector Evaluation We trained a gait detector using DHSs generated using BRIAR training set, and it reaches 91.9%, 86.1% and 88.5% accuracy on BRIAR, CASIA-B and Gait3D respectively. The high accuracy shows that the gait detector is robust to different domains. Visualizations are included in the **supplementary material** section. From

Dataset	Methods	Rank-1	Rank-5	Rank-10	mAP	mINP
CASIA-B	GaitSet [9]	6.90	14.60		4.46	
	GaitGL [27]	8.80	15.70	18.80	5.55	3.16
OUMV-LP	GaitSet [9]	6.10	12.40		4.42	
	GaitGL [27]	16.40	25.80	31.20	13.11	7.28
GREW	GaitSet [9]	16.50	31.10		11.71	
	GaitGL [27]	18.30	31.90	39.20	13.12	7.28
BRIAR	GaitGL [27]	21.50	36.50	42.50	15.16	8.18
	GAR	23.49	37.40	43.40	15.90	8.21
	GADER	25.02	39.18	45.41	16.89	8.62

Table 4: Cross domain evaluation on Gait3D with detector.

Table 1, 2, 3 and 4, the recognition performance increases with the introduction of the detector.

4.4. Ablation Study

To show the impact of each part in our design, we conduct a series of experiments.

RGB modality is sensitive to appearance change. In Table 5, we evaluate the framework only using RGB modality with GaitGL as a feature extraction model, i.e. GaitGL_{RGB}. We observe that it has lower performance than silhouette-based one, i.e. GaitGL, decreasing from 29.77% to 15.69% even only testing on annotated walking sequences set, i.e. Pre-defined, due to its sensitivity to appearance change, but its feature has unique attributes that augment the silhouette feature with a 3.97% improvement.

Ratio and RGB help better silhouette embedding. In the gait recognition model, we evaluate the *ratio attention* and *cross modality distillation*. From Table 6, when we apply cross modality distillation, the recognition accuracy on CL reaches 85% and its verification result increases by 0.52%. As for ratio attention, it improves verification and Rank-1 accuracy under all conditions. Compared to the baseline, our proposed GAR gains a remarkable improvement on verification and Rank-1 in CL from 80.11% and 83.3% to 80.83% and 85.7% respectively, which means the view angle cue from ratio and RGB’s feature space help build a representative embedding.

Mixing gait and non-walking will ruin the feature aggregation. To demonstrate the necessity of gait detector, we first train with all BRIAR training set data, i.e. GaitGL w/ stand, including standing, random walking and structure walking. From Table 5. We see that when standing sequences are involved in the training process, the performance on gait drops, which means that static sequences disturb gait embedding construction. And it is also computationally consuming to apply stand sequence in gait recognition, since there is little temporal information, a 2D model is enough to use. This observation inspires us to develop a detector to filter out static and low-quality silhouettes.

Gait detector purifies gait sequences and improves gait performance. When the gait detector is applied, both models achieve higher recognition results since the detector

Model	Pre-defined	Detected
GaitGL _{RGB} [27]	15.69	14.93
GaitGL w/ stand [27]	33.56	36.46
GaitGL [27]	43.46	45.31
GAR	47.43	50.37

Table 5: Comparison among different models tested on pre-defined gait set and detected set on BRIAR.

Ratio	Cross	R_{NM}	R_{BG}	R_{CL}	$Veri$
✗	✗	97.2	94.1	83.3	80.11
✓	✗	97.4	94.4	85.1	80.42
✗	✓	97.3	94.5	85.0	80.63
✓	✓	97.5	94.5	85.7	80.83

Table 6: Ablation studies on ratio attention and cross modality distillation. The results are shown using recognition accuracy of three probes (R_{NM} , R_{BG} , R_{CL}) and average verification ($Veri$) on CASIA-B.

keeps the silhouette sequences with complete-body and periodic moving patterns. Compared to the Pre-defined gait set, the Detected set further removes sequences with an incomplete body. From Table 1, 2, 3 and 4, we see the potential of detector. Using the same model, GAR, when we exploit a gait detector, almost all performances improve. And this improvement is achieved with little cost, a light-weighted classification network since the DHS is generated by extracting from the input of gait recognition. The well-trained model is robust to domain gaps among different datasets, so it can be directly applied.

5. Conclusion

In this paper, we present a novel end-to-end gait detection and recognition approach to address challenging unconstrained conditions. First, we introduce a gait detector to identify sequences that contain gait movement and with complete body. With the gait detector, we can obtain gait sequences without non-walking frames. And it is convenient to incorporate with most existing backbones, just with an extra step to generate the DHS. Secondly, the gait recognition pipeline utilizes both RGB and silhouette modality to learn robust representation. Notably, we address the silhouette size normalization problem with a simple yet effective ratio attention signal. Additionally, we enhance the silhouette modality embedding through feature distillation from the RGB modality. Such a design helps leverage the well-learned feature space of RGB modality with the robustness of silhouettes and does not require RGB input at test time. Through extensive experiments, we show that our proposed method improves the performance on Gait3D in cross-domain evaluation and achieves SoTA performance in the standard CASIA-B and the more challenging BRIAR datasets.

6. Acknowledgement

This research is based upon work supported in part by the Office of the Director of National Intelligence (ODNI), Intelligence Advanced Research Projects Activity (IARPA), via [2022-21102100005]. The views and conclusions contained herein are those of the authors and should not be interpreted as necessarily representing the official policies, either expressed or implied, of ODNI, IARPA, or the U.S. Government. The U.S. Government is authorized to reproduce and distribute reprints for governmental purposes notwithstanding any copyright annotation therein.

References

- [1] Weizhi An, Rijun Liao, Shiqi Yu, Yongzhen Huang, and Pong C Yuen. Improving gait recognition with 3d pose estimation. In *Chinese Conference on Biometric Recognition*, pages 137–147. Springer, 2018. 1, 2
- [2] Francesco Battistone and Alfredo Petrosino. Tglstm: A time based graph deep learning approach to gait recognition. *Pattern Recognition Letters*, 126:132–138, 2019. 1, 2
- [3] Chiraz Ben Abdelkader, Ross Cutler, and Larry Davis. Stride and cadence as a biometric in automatic person identification and verification. In *Proceedings of Fifth IEEE international conference on automatic face gesture recognition*, pages 372–377. IEEE, 2002. 1, 2
- [4] Csaba Benedek, Bence Gálai, Balázs Nagy, and Zsolt Jankó. Lidar-based gait analysis and activity recognition in a 4d surveillance system. *IEEE Transactions on Circuits and Systems for Video Technology*, 28(1):101–113, 2016. 1
- [5] Aaron F. Bobick and James W. Davis. The recognition of human movement using temporal templates. *IEEE Transactions on pattern analysis and machine intelligence*, 23(3):257–267, 2001. 1, 2
- [6] Aaron F Bobick and Amos Y Johnson. Gait recognition using static, activity-specific parameters. In *Proceedings of the 2001 IEEE Computer Society Conference on Computer Vision and Pattern Recognition. CVPR 2001*, volume 1, pages I–I. IEEE, 2001. 2
- [7] Nikolaos V Boulgouris and Zhiwei X Chi. Human gait recognition based on matching of body components. *Pattern recognition*, 40(6):1763–1770, 2007. 1, 2
- [8] Tianrui Chai, Annan Li, Shaoxiong Zhang, Zilong Li, and Yunhong Wang. Lagrange motion analysis and view embeddings for improved gait recognition. In *Proceedings of the IEEE/CVF Conference on Computer Vision and Pattern Recognition*, pages 20249–20258, 2022. 2, 3, 5, 6, 7
- [9] Hanqing Chao, Yiwei He, Junping Zhang, and Jianfeng Feng. Gaitset: Regarding gait as a set for cross-view gait recognition. In *Proceedings of the AAAI conference on artificial intelligence*, volume 33, pages 8126–8133, 2019. 1, 2, 3, 5, 6, 8
- [10] Changhong Chen, Jimin Liang, Heng Zhao, Haihong Hu, and Jie Tian. Frame difference energy image for gait recognition with incomplete silhouettes. *Pattern Recognition Letters*, 30(11):977–984, 2009. 1, 2
- [11] David Cornett III, Joel Brogan, Nell Barber, Deniz Aykac, Seth Baird, Nick Burchfield, Carl Dukes, Andrew Duncan, Regina Ferrell, Jim Goddard, et al. Expanding accurate person recognition to new altitudes and ranges: The BRIAR dataset. *arXiv preprint arXiv:2211.01917*, 2022. 1, 5, 7
- [12] Silvia Del Din, Morad Elshehabi, Brook Galna, Markus A Hobert, Elke Warmerdam, Ulrike Suenkel, Kathrin Brockmann, Florian Metzger, Clint Hansen, Daniela Berg, et al. Gait analysis with wearables predicts conversion to parkinson disease. *Annals of neurology*, 86(3):357–367, 2019. 1
- [13] Chao Fan, Yunjie Peng, Chunshui Cao, Xu Liu, Saihui Hou, Jiannan Chi, Yongzhen Huang, Qing Li, and Zhiqiang He. Gaitpart: Temporal part-based model for gait recognition. In

- Proceedings of the IEEE/CVF conference on computer vision and pattern recognition*, pages 14225–14233, 2020. [2](#), [3](#), [5](#), [6](#), [7](#)
- [14] Yuxiang Guo, Cheng Peng, Chun Pong Lau, and Rama Chellappa. Multi-modal human authentication using silhouettes, gait and rgb. *arXiv preprint arXiv:2210.04050*, 2022. [2](#)
- [15] Abdenour Hadid, Mohammad Ghahramani, Vili Kellokumpu, Matti Pietikäinen, John Bustard, and Mark Nixon. Can gait biometrics be spoofed? In *Proceedings of the 21st international conference on pattern recognition (ICPR2012)*, pages 3280–3283. IEEE, 2012. [1](#)
- [16] Jinguang Han and Bir Bhanu. Individual recognition using gait energy image. *IEEE transactions on pattern analysis and machine intelligence*, 28(2):316–322, 2005. [1](#), [2](#)
- [17] Elad Hoffer and Nir Ailon. Deep metric learning using triplet network. In Yoshua Bengio and Yann LeCun, editors, *3rd International Conference on Learning Representations, ICLR 2015, San Diego, CA, USA, May 7-9, 2015, Workshop Track Proceedings*, 2015. [3](#), [5](#)
- [18] Emdad Hossain and Girija Chetty. Multimodal feature learning for gait biometric based human identity recognition. In *International Conference on Neural Information Processing*, pages 721–728. Springer, 2013. [2](#)
- [19] Saihui Hou, Xu Liu, Chunshui Cao, and Yongzhen Huang. Gait quality aware network: Toward the interpretability of silhouette-based gait recognition. *IEEE Transactions on Neural Networks and Learning Systems*, pages 1–11, 2022. [3](#)
- [20] Xiaohu Huang, Duowang Zhu, Hao Wang, Xinggong Wang, Bo Yang, Botao He, Wenyu Liu, and Bin Feng. Context-sensitive temporal feature learning for gait recognition. In *Proceedings of the IEEE/CVF International Conference on Computer Vision*, pages 12909–12918, 2021. [6](#), [7](#)
- [21] Zhen Huang, Dixiu Xue, Xu Shen, Xinmei Tian, Houqiang Li, Jianqiang Huang, and Xian-Sheng Hua. 3d local convolutional neural networks for gait recognition. In *Proceedings of the IEEE/CVF International Conference on Computer Vision*, pages 14920–14929, 2021. [6](#), [7](#)
- [22] Amit Kale, Aravind Sundaresan, AN Rajagopalan, Naresh P Cuntoor, Amit K Roy-Chowdhury, Volker Kruger, and Rama Chellappa. Identification of humans using gait. *IEEE Transactions on image processing*, 13(9):1163–1173, 2004. [2](#)
- [23] Chun Pong Lau, Carlos D Castillo, and Rama Chellappa. Atfacegan: Single face semantic aware image restoration and recognition from atmospheric turbulence. *IEEE Transactions on Biometrics, Behavior, and Identity Science*, 3(2):240–251, 2021. [3](#)
- [24] Xuelong Li, Stephen J Maybank, Shuicheng Yan, Dacheng Tao, and Dong Xu. Gait components and their application to gender recognition. *IEEE Transactions on Systems, Man, and Cybernetics, Part C (Applications and Reviews)*, 38(2):145–155, 2008. [1](#), [2](#)
- [25] Junhao Liang, Chao Fan, Saihui Hou, Chuanfu Shen, Yongzhen Huang, and Shiqi Yu. Gaitedge: Beyond plain end-to-end gait recognition for better practicality. *arXiv preprint arXiv:2203.03972*, 2022. [3](#), [5](#)
- [26] Rijun Liao, Chunshui Cao, Edel B Garcia, Shiqi Yu, and Yongzhen Huang. Pose-based temporal-spatial network (ptsn) for gait recognition with carrying and clothing variations. In *Chinese conference on biometric recognition*, pages 474–483. Springer, 2017. [1](#), [2](#)
- [27] Beibei Lin, Shunli Zhang, and Xin Yu. Gait recognition via effective global-local feature representation and local temporal aggregation. In *Proceedings of the IEEE/CVF International Conference on Computer Vision*, pages 14648–14656, 2021. [1](#), [2](#), [3](#), [5](#), [6](#), [7](#), [8](#)
- [28] Jianyi Liu and Nanning Zheng. Gait history image: a novel temporal template for gait recognition. In *2007 IEEE international conference on multimedia and expo*, pages 663–666. IEEE, 2007. [1](#), [2](#)
- [29] Zongyi Liu, Laura Malave, Adebola Osuntogun, Preksha Sudhakar, and Sudeep Sarkar. Toward understanding the limits of gait recognition. In *Biometric Technology for Human Identification*, volume 5404, pages 195–205. SPIE, 2004. [2](#)
- [30] Zongyi Liu and Sudeep Sarkar. Improved gait recognition by gait dynamics normalization. *IEEE Transactions on Pattern Analysis and Machine Intelligence*, 28(6):863–876, 2006. [2](#)
- [31] Jason M Nash, John N Carter, and Mark S Nixon. Dynamic feature extraction via the velocity hough transform. *Pattern Recognition Letters*, 18(10):1035–1047, 1997. [2](#)
- [32] Sourabh A Niyogi and Edward H Adelson. Analyzing gait with spatiotemporal surfaces. In *Proceedings of 1994 IEEE Workshop on Motion of Non-rigid and Articulated Objects*, pages 64–69. IEEE, 1994. [2](#), [4](#)
- [33] Adam Paszke, Sam Gross, Francisco Massa, Adam Lerer, James Bradbury, Gregory Chanan, Trevor Killeen, Zeming Lin, Natalia Gimelshein, Luca Antiga, et al. Pytorch: An imperative style, high-performance deep learning library. *Advances in neural information processing systems*, 32, 2019. [6](#)
- [34] Yang Ran, Qinfen Zheng, Rama Chellappa, and Thomas M Strat. Applications of a simple characterization of human gait in surveillance. *IEEE Transactions on Systems, Man, and Cybernetics, Part B (Cybernetics)*, 40(4):1009–1020, 2010. [2](#), [4](#)
- [35] Sudeep Sarkar, P Jonathon Phillips, Zongyi Liu, Isidro Robledo Vega, Patrick Grother, and Kevin W Bowyer. The humanid gait challenge problem: Data sets, performance, and analysis. *IEEE transactions on pattern analysis and machine intelligence*, 27(2):162–177, 2005. [1](#), [2](#)
- [36] Alireza Sepas-Moghaddam and Ali Etemad. Deep gait recognition: A survey. *IEEE transactions on pattern analysis and machine intelligence*, 45(1):264–284, 2022. [1](#)
- [37] Chuanfu Shen, Shiqi Yu, Jilong Wang, George Q Huang, and Liang Wang. A comprehensive survey on deep gait recognition: algorithms, datasets and challenges. *arXiv preprint arXiv:2206.13732*, 2022. [1](#)
- [38] Kohei Shiraga, Yasushi Makihara, Daigo Muramatsu, Tomio Echigo, and Yasushi Yagi. Geinet: View-invariant gait recognition using a convolutional neural network. In *2016 international conference on biometrics (ICB)*, pages 1–8. IEEE, 2016. [2](#)
- [39] Noriko Takemura, Yasushi Makihara, Daigo Muramatsu, Tomio Echigo, and Yasushi Yagi. Multi-view large population gait dataset and its performance evaluation for cross-

- view gait recognition. *IPSN Transactions on Computer Vision and Applications*, 10(1):1–14, 2018. 3, 6
- [40] Rawesak Tanawongsuwan and Aaron Bobick. Gait recognition from time-normalized joint-angle trajectories in the walking plane. In *Proceedings of the 2001 IEEE Computer Society Conference on Computer Vision and Pattern Recognition. CVPR 2001*, volume 2, pages II–II. IEEE, 2001. 2
- [41] Liang Wang, Huazhong Ning, Tieniu Tan, and Weiming Hu. Fusion of static and dynamic body biometrics for gait recognition. *IEEE Transactions on circuits and systems for video technology*, 14(2):149–158, 2004. 2
- [42] Yuxin Wu, Alexander Kirillov, Francisco Massa, Wan-Yen Lo, and Ross Girshick. Detectron2. <https://github.com/facebookresearch/detectron2>, 2019. 3, 6
- [43] Zifeng Wu, Yongzhen Huang, Liang Wang, Xiaogang Wang, and Tieniu Tan. A comprehensive study on cross-view gait based human identification with deep cnns. *IEEE transactions on pattern analysis and machine intelligence*, 39(2):209–226, 2016. 2, 6
- [44] Junfei Xiao, Longlong Jing, Lin Zhang, Ju He, Qi She, Zongwei Zhou, Alan Yuille, and Yingwei Li. Learning from temporal gradient for semi-supervised action recognition. In *Proceedings of the IEEE/CVF Conference on Computer Vision and Pattern Recognition*, pages 3252–3262, 2022. 5
- [45] Rajeev Yasarla and Vishal M Patel. Learning to restore images degraded by atmospheric turbulence using uncertainty. In *2021 IEEE International Conference on Image Processing (ICIP)*, pages 1694–1698. IEEE, 2021. 3
- [46] Jang-Hee Yoo, Doosung Hwang, Ki-Young Moon, and Mark S Nixon. Automated human recognition by gait using neural network. In *2008 First Workshops on Image Processing Theory, Tools and Applications*, pages 1–6. IEEE, 2008. 1, 2
- [47] Shiqi Yu, Daoliang Tan, and Tieniu Tan. A framework for evaluating the effect of view angle, clothing and carrying condition on gait recognition. In *18th International Conference on Pattern Recognition (ICPR'06)*, volume 4, pages 441–444. IEEE, 2006. 3, 6
- [48] Erhu Zhang, Yongwei Zhao, and Wei Xiong. Active energy image plus 2dlpp for gait recognition. *Signal Processing*, 90(7):2295–2302, 2010. 1, 2
- [49] Yuqi Zhang, Yongzhen Huang, Shiqi Yu, and Liang Wang. Cross-view gait recognition by discriminative feature learning. *IEEE Transactions on Image Processing*, 29:1001–1015, 2019. 2
- [50] Jinkai Zheng, Xinchun Liu, Wu Liu, Lingxiao He, Chenggang Yan, and Tao Mei. Gait recognition in the wild with dense 3d representations and a benchmark. In *Proceedings of the IEEE/CVF Conference on Computer Vision and Pattern Recognition*, pages 20228–20237, 2022. 1, 3, 6, 7
- [51] Zheng Zhu, Xianda Guo, Tian Yang, Junjie Huang, Jiankang Deng, Guan Huang, Dalong Du, Jiwen Lu, and Jie Zhou. Gait recognition in the wild: A benchmark. In *Proceedings of the IEEE/CVF international conference on computer vision*, pages 14789–14799, 2021. 1, 3